Please cite as,

Kondou, C., BaBa, D., Mishima, F., Koyama, S., "Flow Boiling of Non-Azeotropic Mixture R32/R1234ze(E) in Horizontal Microfin Tubes", Int. J. Refrig., 36, 2366-2378, (2013).

Flow boiling of non-azeotropic mixture R32/R1234ze(E) in horizontal microfin tubes

Authors: Chieko Kondou*[1], Daisuke BaBa[1], Fumiya Mishima[1], Shigeru Koyama[1, 2]

Affiliations:

1, Interdisciplinary Graduate School of Engineering Sciences, Kyushu University, 6-1 Kasuga-koen, Kasuga, Fukuoka 816-8580, Japan

2, International Institute for Carbon-Neutral Energy Research (WPI-I2CNER), Kyushu University, 6-1 Kasuga-koen, Kasuga, Fukuoka 816-8580, Japan

* Corresponding author.

Tel.: +81 92 583 7832

Fax: +81 92 583 7833

E-mail address: kondo.chieko.162@m.kyushu-u.ac.jp (C. Kondou)

Abstract:

Flow boiling of a potential refrigerant R32/R1234ze(E) in a horizontal microfin tube of 5.21 mm inner diameter is experimentally investigated. The heat transfer coefficient (HTC) and pressure drop are measured at a saturation temperature of 10 °C, heat fluxes of 10 and 15 kW m^{-2}, and mass velocities from 150 to 400 kg $m^{-2}s^{-1}$. The HTC of R1234ze(E) is lower than that of R32. Degradation in the HTC of the R32/R1234ze(E) mixture is significant; the HTC is even lower than that of R1234ze(E). The HTC is minimized at the composition 0.2/0.8 by mass, where the temperature glide and the mass fraction distribution are maximized. A predicting correlation based on Momoki et al. (1995) associated with the correction methods of Thome (1981) to consider the mass transfer resistance and Stephan (1992) to consider the additionally required sensible heat is proposed and validated with the experimental results.

Keywords:

flow boiling; heat transfer; pressure drop; microfin tube; zeotropic mixture; low GWP

Nomenclature

A_{act}	actual interior surface area (m^2)
C_{ir}	empirical constant related to interfacial resistance (-)
Cp	isobaric heat capacity ($J\ kg^{-1}K^{-1}$)
D_{12}	mutual diffusion coefficient ($m^2\ s^{-1}$)
D_{be}	bubble departure diameter (m)
D_o	outer diameter (m)
F	Reynolds number factor (m)
G	mass velocity based on ($kg\ m^{-2}s^{-1}$)
Ja^*	modified Jacob number (-)
N_{Sn}	Scriven number (-)
P	pressure (Pa)
Pr	Prandtl number (-)
Q	heat transfer rate (W)
La	Laplace constant (-)
Re	Reynolds number (-)
T	temperature (^oC)
V	volumetric flow rate ($m^3\ s^{-1}$)
W	mass flow rate ($kg\ s^{-1}$)
X	mass fraction in liquid phase or circulation composition by mass (-)
$\tilde{X}$	mole fraction in liquid phase (-)

$\tilde{Y}$	mole fraction in vapor phase (-)
a	thermal diffusivity ($m^2\ s^{-1}$)
d_{eq}	equivalent inner diameter (m)
h	specific enthalpy ($J\ kg^{-1}$)
q	heat flux ($W\ m^{-2}$)
x	thermodynamic vapor quality (-)

Greek symbols

X_{tt}	Lockhart-Martinelli parameter for turbulent flow (-)
	$=[(1 - x) / x]^{0.9}(\rho_V / \rho_L)^{0.5}(\mu_L / \mu_V)^{0.1}$
ΔZ	tube length (m)
Δh_{LV}	latent heat of vaporization ($J\ kg^{-1}$)
α	heat transfer coefficient ($W\ m^{-2}K^{-1}$)
β	lead angle (rad)
ε	bias (-)
η_A	surface enlargement ratio (-)
λ	thermal conductivity ($W\ m^{-1}K^{-1}$)
μ	viscosity (Pa·s)
ρ	density ($kg\ m^{-3}$)
σ	surface tension ($N\ m^{-2}$)
σ_{dev}	standard deviation (-)

Subscripts

1	the more volatile component, R32
2	the less volatile component, R1234ze(E)
AH	after heater
DP	distance between pressure taps
H2O	water
L	liquid
R32	R32
TP	two phase
TS	test section
V	vapor
max	maximum
min	minimum
act	actual
bub	bubble point, or bubble
cal	calculation
cv	forced convection contribution
dew	dew point
eq	equivalent
exp	experiment

i	inlet
loss	heat loss to ambient
mix	mixture
nb	nucleate boiling contribution
o	outlet
pb	pool boiling
r	refrigerant
sat	saturation
tube	test tube
wi	interior tube wall
wo	exterior tube wall
α	active heat transfer length

1. Introduction

R1234ze(E), trans-1,3,3,3-tetrafluoro-1-propene, is anticipated to be an environment-friendly refrigerant for air conditioners because of its zero ozone depletion potential (ODP) and extremely low (less than 10) global warming potential (GWP). However, in recent studies, it was found that the coefficient of performance (COP) and the capacity of heat pump cycles using R1234ze(E) are significantly lower than those of the most widely used refrigerant, R410A. The main causes are the small latent heat and vapor density of R1234ze(E). To improve the COP and capacity, in the latest literature (e.g., Koyama et al, 2010a), it was attempted to blend R1234ze(E) into another refrigerant, R32. Because of its large latent heat and relatively

low GWP of 675, R32 was selected as a second component to be blended with R1234ze(E). As the result of their drop-in test with R32/R1234ze(E) 0.5/0.5 by mass, Koyama et al. (2010a) concluded that the tested binary mixture achieved a superior COP at some operating conditions, and this binary mixture is the most promising candidate to replace R410A.

As mentioned in many previous studies (e.g., Jacobs and Kruse, 1978; McLinden and Radermacher, 1987), exergy loss in heat exchangers can be minimized by utilizing the temperature glide of zeotropic mixtures. Whereas, as investigated in numerous heat transfer studies, there is severe degradation in the heat transfer coefficient (HTC) due to the volatility difference.

For instance, the flow boiling HTC of binary mixtures R152a/R13B1, R22/R114, and R12/R152a in a horizontal smooth tube of 9 mm inner diameter (ID) were experimentally provided by Ross et al. (1987), and Jung et al. (1989a, 1989b). Similarly, other binary mixtures R846/R12 and R116/134a were tested with a smooth tube of 14 mm ID by Niederkrüger et al. (1992, 1994), and Wettermann and Steiner (2000). Furthermore, HTC data of R32/R134a and R290/R600a in a smooth tube of 7.7 mm ID were reported by Shin et al. (1997). Thus, abundant variations of the combinations were tested for horizontal smooth tubes. The experimental results showed a drastic decrease in the HTC of the zeotropic binary mixtures compared with the components. The cause of this heat transfer degradation is typically called mass transfer resistance. As the discussion for the roles of the temperature glide and the concentration distribution in the mass transfer resistance advanced, a heat transfer model was developed. Murata and Hashizume (1993), Niederküger and Steiner (1994), Jung and Radermacher (1993), Takamatsu et al. (1993a, 1993b), and Kandlikar (1998a, 1998b) proposed a prediction method of the HTC for horizontal microfin tubes. Most of the works introduced above were comprehensively reviewed by Celata et al. (1994). More recently, Hossain et al. (2013) reported HTC data for the low GWP refrigerant mixture R1234ze(E)/R32 that is the same combination investigated in this paper. With this binary mixture, they confirmed the typical effects of the mass transfer resistance for a horizontal smooth tube of 4.35 mm ID.

Very often the magnitude of the mass transfer resistance is much larger than the argumentation of the flow regime or the enhancement by microfins. Although microfin tubes have been widely applied in heat pump systems to improve the COP and to downsize heat exchangers for decades, the advantage can be canceled out by the mass transfer resistance in zeotropic mixtures. Despite this, to the best of the author's knowledge, the available data seem inadequate for the HTC and pressure drop predictions of zeotropic binary mixtures in horizontal microfin tubes. Koyama et al. (1987) experimentally determined the HTC of R22/R114 in a microfin tube of 8.32 mm ID. Yoshida et al. (1990, 1993) measured the HTC of R22/R114 in a microfin tube of 11.6 mm ID. Torikoshi and Ebisu (1994) measured the overall HTC from the evaporator inlet to outlet for R32/R134a in a microfin tube of 6.4 mm ID. Cho et al. (2010) reported on R744/R290 with a 4.13 mm ID for the tube, but they defined the HTC with the bubble point and not the local saturation temperature.

As mentioned above, it is practically important to find the optimal composition that determines the magnitude of the heat transfer degradation. Based upon the above literature review, the HTC and pressure drop of the zeotropic mixture R32/R1234ze(E) of various compositions are experimentally investigated in this study, with the highly accurate thermodynamic properties provided by a substantially improved equation of state and mixing model.

2. Experiment

2.1 Experimental apparatus

Figure 1 describes the arrangement of an experimental apparatus used in this study. The refrigerant flow rate and pressure are adjusted by the speed of a compressor (1), the temperature in a condenser (3), and the open width of a solenoid expansion valve (6). The inlet vapor quality at a test section (8) is adjusted by an electric heater (7). In the mixing chambers, the refrigerant pressures and bulk-mean-temperatures are measured to find the enthalpies. At a sampling port (11), approximately 1 cc of circulating subcooled liquid is instantaneously sampled. The composition of

the sampled refrigerants is determined by a thermal conductivity detector (TCD) gas chromatograph. The composition shift between circulation and charge were reported (e.g., Haberschill et al., 2002; Fukuda et al., 2012), and a similar composition shift was found over the validation test. Because the reversal in the measured tube wall temperature and the refrigerant saturation temperature was yielded when the saturation temperature was evaluated at the charged composition, the refrigerant properties are evaluated at the composition of the sampled refrigerant.

Figure 2 illustrates two subsections of the test section divided into four subsections. A test microfin tube (1) of 2216 mm total length, made of copper, is surrounded by four water jackets (2) of counter flow configuration. Each water jacket of 414 mm active heating length carries out the function of the subsection to measure the average HTC. The wall temperature is measured by thermocouples (3) embedded in the top, bottom, right, and left of the exterior test tube wall at the center of heating length. The bulk-mean-temperature of the inlet and outlet water is measured in the mixing chambers (6). The pressure drop between pressure-ports of 0.8 mm diameter, bored in the test microfin tube at intervals of 554 mm, is measured by a differential pressure transducer (4). Figures 3 (a) and (b) are the microscopic pictures of 45 ^{o} and 90 ^{o} cut surfaces of the test microfin tube.

Table 1 specifies the dimensions of the test microfin tube. The equivalent inner diameter d_{eq} is the inner diameter of a smooth tube having the same internal free flow volume. Surface enlargement is the ratio of the actual heat transfer area to the surface area enveloped at the equivalent inner diameter. Refrigerant mass velocity is defined at the actual free flow cross-sectional area ($d_{eq}^2 \pi$ / 4) in this study. Heat flux and HTC are defined at the actual heat transfer area ($d_{eq} \eta_A \Delta Z_\alpha$), but not the heat transfer area of the equivalent smooth tube.

Table 2 lists the measurement uncertainties obtained from the results of two calibration standard deviations, the resolution of data loggers and calibration tools, and the stability of the excitation voltages. The combined measured uncertainties for the HTC are calculated from the uncertainties by means of the square-root rule (Taylor 1982; Moffat,

1988). The calculation procedure is specified in Appendix.

2.2 Data reduction procedure

Figure 4 illustrates the measured values and the data reduction procedure. The specific enthalpy of the superheated vapor at the after-heater outlet, h_{AHo}, is calculated from the refrigerant pressure, bulk-mean temperature, and circulation composition. In the test section, the inlet and outlet refrigerant enthalpies of each subsection are obtained from the water side heat balance through the after-heater and subsections.

$$\left.\begin{aligned} h_1 &= h_{\mathrm{AHo}} - \left(Q_{\mathrm{H2O,AH}}/W_{\mathrm{r}}\right) = h_{\mathrm{AHo}} - \left[\rho_{\mathrm{H2O}} Cp_{\mathrm{H2O}} V_{\mathrm{H2O,\,AH}} \left(T_{\mathrm{H2O,AHi}} - T_{\mathrm{H2O,AHo}}\right) - Q_{\mathrm{loss,AH}}\right] \Big/ \left(G_{\mathrm{r}}\, {d_{\mathrm{eq}}}^2 \pi/4\right) \\ h_2 &= h_1 - \left(Q_{\mathrm{H2O,1}}/W_{\mathrm{r}}\right) = h_1 - \left[\rho_{\mathrm{H2O}} Cp_{\mathrm{H2O}} V_{\mathrm{H2O,\,TS}} \left(T_{\mathrm{H2O,\,1i}} - T_{\mathrm{H2O,\,1o}}\right) - Q_{\mathrm{loss,\,TS}}\right] \Big/ \left(G_{\mathrm{r}}\, {d_{\mathrm{eq}}}^2 \pi/4\right) \\ &\vdots \qquad\qquad\qquad\qquad \vdots \\ h_5 &= h_4 - \left(Q_{\mathrm{H2O,4}}/W_{\mathrm{r}}\right) = h_4 - \left[\rho_{\mathrm{H2O}} Cp_{\mathrm{H2O}} V_{\mathrm{H2O,\,TS}} \left(T_{\mathrm{H2O,\,4i}} - T_{\mathrm{H2O,\,4o}}\right) - Q_{\mathrm{loss,\,TS}}\right] \Big/ \left(G_{\mathrm{r}}\, {d_{\mathrm{eq}}}^2 \pi/4\right) \end{aligned}\right\} \quad (1)$$

where, W_{r} is the refrigerant mass flow rate. ρ_{H2O}, Cp_{H2O}, and V_{H2O} are the density, isobaric specific heat, and volumetric flow rate of the heating water, respectively. Q_{loss} is the heat loss to the ambient air through the insulation, which is correlated with temperature difference between ambient air and the heating water by the preliminary test. For the typical test condition, the heat loss Q_{loss} is typically 2% (approximately 3 W for a subsection) of the heat transfer rate $Q_{\mathrm{H2O,TS}}$. Assuming an equilibrium state, the representative refrigerant temperature, T_{r}, and vapor quality, x, in a subsection are calculated from the pressure, enthalpy, and circulation composition, i.e., the R32 mass fraction of the sampled liquid, X_{R32}. For instance, the representative refrigerant temperature and vapor quality in the subsection 1 are given as,

$$\left.\begin{aligned} T_{\mathrm{r,1}} &= \left[T_{\mathrm{r,1i}}\left(P_{\mathrm{AHi}}, h_1, X_{\mathrm{R32}}\right)_{\mathrm{equilibrium}} + T_{\mathrm{r,1o}}\left(P_2, h_2, X_{\mathrm{R32}}\right)_{\mathrm{equilibrium}}\right]/2 \\ x_1 &= \left[x_{\mathrm{1i}}\left(P_{\mathrm{AHi}}, h_1, X_{\mathrm{R32}}\right)_{\mathrm{equilibrium}} + x_{\mathrm{1o}}\left(P_2, h_2, X_{\mathrm{R32}}\right)_{\mathrm{equilibrium}}\right]/2 \end{aligned}\right\} \quad (2)$$

The average HTC, α, and heat flux, q_{act}, based on the actual heat transfer area, A_{act}, in a subsection are given as

$$\alpha = q_{\mathrm{act}} / \left(T_{\mathrm{wi}} - T_{\mathrm{r}} \right)$$
$$q_{\mathrm{act}} = \frac{Q_{\mathrm{H2O}}}{A_{\mathrm{act}}} = \frac{V_{\mathrm{H2O}} \rho_{\mathrm{H2O}} Cp_{\mathrm{H2O}} \left(T_{\mathrm{H2O,i}} - T_{\mathrm{H2O,o}} \right) - Q_{\mathrm{loss,\ TS}}}{d_{\mathrm{eq}} \pi \eta_{\mathrm{A}} \Delta Z_{\alpha}} \tag{3}$$

ΔZ_{α} is the active heating length 0.414 m. The tube wall temperature, T_{wi}, at the equivalent inner diameter, d_{eq}, is found from the measured temperatures of the exterior tube wall, T_{wo}, with due consideration of Fourier's law.

$$T_{\mathrm{wi}} = \left(\frac{T_{\mathrm{wo,\ top}} + T_{\mathrm{wo,\ bottom}} + T_{\mathrm{wo,\ right}} + T_{\mathrm{wo,\ left}}}{4} \right) - \ln\left(\frac{D_{\mathrm{o}}}{d_{\mathrm{eq}}} \right) \frac{Q_{\mathrm{H2O}}}{2\pi \lambda_{\mathrm{tube}} \Delta Z_{\alpha}} \tag{4}$$

On the other hand, pressure drop through each subsection is given as,

$$\begin{aligned} \left(\Delta P / \Delta Z \right)_1 &= \left(\Delta P_{02} - \Delta P_{01} \right) / \Delta Z_{\mathrm{DP},1} \\ &\vdots \\ \left(\Delta P / \Delta Z \right)_4 &= \left(\Delta P_{00} - \Delta P_{04} \right) / \Delta Z_{\mathrm{DP},4} \end{aligned} \tag{5}$$

where ΔZ_{DP} is the interval of pressure ports 0.554 m.

The refrigerant properties in this study are calculated by Refprop (Lemmon et al. 2010) coupled with the R1234ze(E) database of the version updated on June 2012. It should be noted that the mixing parameters for R32/R1234ze(E) were optimized by Akasaka (2012) to fit the phase equilibria data experimentally provided by Koyama et al. (2010b).

3. Results and discussion

Figures 5 (a), (b), (c), and (d) plot the HTC of R1234ze(E), R32/R1234ze(E) (0.2/0.8 by mass), R32/R1234ze(E) (0.5/0.5 by mass), and R32, respectively. The horizontal axes show the vapor quality and the vertical axes show the HTC based on the actual heat transfer area. Symbol markers show the experimental HTC data, with vertical bars indicating the combined measurement uncertainty and horizontal bars indicating the vapor quality change in a

subsection. Solid and dashed lines are the predicted HTC by the correlations of Mori et al. (2002) for the single components and of Cavallini et al. (1998) for the mixture.

3.1 HTC of single components R1234ze(E) and R32

Comparing Figures 5 (a) and (d), the HTC of R32 is approximately twice as high relative to R1234ze(E), particularly at vapor qualities less than 0.3. This can be explained by the 1.7 times higher liquid thermal conductivity and 1.66 times larger latent heat of R32, relative to those of R1234ze(E). It appears that the well-known HTC degradation "dry-out" occurs at relatively lower vapor qualities in R1234ze(E) flow. This is most likely because of the higher vapor velocity, due to the half as dense R1234ze(E) vapor. Comparing the lines to the symbols, the experimental HTC satisfactorily agrees with the prediction. This validates the present experimental method. Some other correlations are assessed for single components, below.

Table 3 compares the experimental HTC and predicted HTC by correlations proposed for other single components by Momoki et al. (1995), Thome et al. (1997), Mori et al. (2002), Yun et al. (2002), and Chamra and Mago (2007). Additionally, the correlations proposed for binary mixtures by Cavallini et al. (1998) and Murata (1996) are compared under the hypothesis that the binary mixture eventuates in single components at the mass fractions 0 and 1. The HTC defined with the equivalent or fin tip diameter in those correlations is transcribed to the basis of the actual heat transfer area. To eliminate the HTC data in the dry-out region, 44 and 90 points of HTC data are selected for R1234ze(E) and R32, respectively. The degree of the agreement is quantified with the average bias, $\bar{\varepsilon}$, and two standard deviations from the average, $2\sigma_{\mathrm{dev}}$.

$$\bar{\varepsilon} = \frac{1}{n}\sum_{j=1}^{n}\varepsilon_j = \frac{1}{n}\sum_{j=1}^{n}\left[\left(\alpha_{\mathrm{cal},j} - \alpha_{\mathrm{exp},j}\right)/\alpha_{\mathrm{exp},j}\right], \quad 2\sigma_{\mathrm{dev}} = 2\sqrt{\frac{1}{n-1}\sum_{j=1}^{n}\left(\varepsilon_j - \bar{\varepsilon}\right)^2} \tag{6}$$

As shown in Table 3, the selected correlations reasonably agree with the experimental R1234ze(E), except for the correlation of Chamra and Mago (2007). For R32, all the selected correlations, especially the three correlations proposed for single components, show good agreement. This assessment also verifies the present experimental method. The effect of the lubricant oil seems negligible.

3.2 HTC of binary mixture R32/R1234ze(E)

Figures 5 (b) and (c) plot the HTC of the binary mixtures R32/R1234ze(E) at the circulation compositions 0.2/0.8 and 0.5/0.5 by mass, respectively. Solid lines are the predicted HTC by Cavallini et al. (1998). The HTC in the vapor quality range from 0 to 0.4, where the nucleate boiling contribution is dominant, is larger at 0.5/0.5 by mass than that at 0.2/0.8. With an increasing mass fraction of R32, the contribution of R32 seems to be aiding heat transfer. On the other hand, in the vapor quality range above 0.4, where the forced convection contribution is dominant, the HTC at 0.5/0.5 by mass is slightly lower than that at 0.2/0.8 by mass. Because the vapor velocity of R1234ze(E) is higher than that of R32 at the fixed mass velocity and the temperature, this contribution is more explicit in the HTC at 0.2/0.8 by mass.

Table 4 compares the experimental HTC and predicted HTC by Murata (1996), Cavallini et al. (1998), and Chamra and Mago (2007) for the mixture R32/R1234ze(E). The bias and standard deviation of Cavallini et al. (1998) are acceptably small. As also shown in Figures 5 (b) and (c), this correlation predicts well the HTC at vapor qualities beyond 0.5. Nevertheless, the deviation at vapor quality less than 0.5 is still considerable.

3.3 Heat transfer degradation by volatility difference

Figure 6 shows the phase equilibrium of R32/R1234ze(E) (0.5/0.5 by mass) at 0.8 MPa to illustrate the volatility difference. For a given circulation composition of $\tilde{X}_{x=0}$, the bulk mole fraction of the liquid phase alone changes from

$\tilde{X}_{x=0}$ to $\tilde{X}_{x=1}$ with temperature rising along the bubble point curve. The fraction of the vapor phase alone changes from $\tilde{Y}_{x=0}$ to $\tilde{Y}_{x=1}$ along the dew point curve, and then the superheated vapor eventually exits from the heat exchangers. By this volatility difference, through the evaporation process, the liquid phase becomes richer in the less volatile component R1234ze(E), while the vapor phase becomes richer in the more volatile component R32. As shown in Figure 6, the mole fraction of the vapor differs from 0.16 to 0.25 at the vapor quality from 0 to 1 for the fixed circulation composition 0.5/0.5 by mass. Thus, a strong mole fraction gradient is formed over the liquid-vapor interface. Therefore, at the liquid-vapor interface of the liquid side, the saturation temperature is locally increased in the concentration boundary layer rich in the less volatile component. This requires more heating for evaporation. Further, the less volatile component diffuses away from the liquid surface. As a consequence of the local saturation temperature rising and the counter diffusion, the mass transfer (i.e., evaporation) is resisted at the bubble surface.

At the boiling site, as evaporation processes, the superheated sublayer adjacent to the tube wall is filled with the less volatile component. This reinforces the above mentioned mass transfer resistance, and the nucleate boiling is fully suppressed. However, as shown in Figure 5, the heat transfer degradation is obvious at higher vapor qualities, where the nuclear boiling is diminished and convection dominantly contributes to the heat transfer. The mole fraction gradient is also formed at the surface of the liquid phase. From the local saturation temperature rising and counter diffusion, the convective mass transfer is resisted. Additionally, the departed bubbles are most likely affected by this interfacial mass transfer resistance. This is why heat transfer degradation is distinct not only in the nuclear boiling region but also the convective evaporation region.

In flow boiling of zeotropic mixtures, the saturation temperature increases along flow paths. Consequently, an additional heat amount is required for heating the vapor flow up to the saturation temperature (vaporized upstream at the lower saturation temperature) as stated by Butterworth (1981) and also by Stephan (1992). Therefore, a

considerably large thermal resistance is generated in the core vapor flow. This is also one reason that the heat transfer degradation is distinct for the entire range of vapor quality.

Figure 7 (a) shows the variation of the temperature glide and the mole fraction difference of liquid to vapor. Figures 7 (b) and (c) show the variation of the HTC related to the mass fraction at mass velocities approximately 200 and 400 $\mathrm{kg\,m^{-2}s^{-1}}$. As reviewed by Celata et al. (1994), numerous data of zeotropic flow boiling in smooth tubes suggest the relativity of HTC to the temperature glide, which represents the additional sensible heat required in the downstream vapor phase, and to the liquid-to-vapor mole fraction difference, which represents the suppression of nucleate boiling and the interfacial mass transfer resistance. The present data for the HTC in the microfin tube show a similar relativity. The experimental HTC is minimized at the R32 mass fraction of approximately 0.2. More specifically, the minimum HTC appears at the mass fractions 0.15, 0.2, and 0.3 for vapor quality 0.2, 0.5 and 0.8, respectively. These fractions correspond to the conditions where the liquid-to-vapor mole fraction difference is maximized at each vapor quality.

3.4 Prediction method for HTC of mixtures in microfin tubes

To consider this thermal resistance that occurs in the vapor core, the HTC from the tube wall to the core vapor flow is given by,

$$\alpha = \left[\frac{1}{\alpha_{\mathrm{V}}} \left(x Cp_{\mathrm{V}} \left. \frac{dT_{\mathrm{sat}}}{dh} \right|_{p} \right) + \frac{1 + C_{\mathrm{ir}} \left(\tilde{Y}_1 - \tilde{X}_1 \right)}{\left(\alpha_{\mathrm{cv}} + \alpha_{\mathrm{nb,mix}} \right)} \right]^{-1} \tag{7}$$

where,

$$\alpha_{\mathrm{V}} = \left(\frac{\lambda_{\mathrm{V}}}{d_{\mathrm{eq}}} \right) 0.023 \left(\frac{G_{\mathrm{r}} d_{\mathrm{eq}}}{\mu_{\mathrm{V}}} \right)^{0.8} \mathrm{Pr}^{\frac{1}{3}},$$
$$\left. \frac{dT_{\mathrm{sat}}}{dh} \right|_{p} \cong \frac{T_{\mathrm{dew}} - T_{\mathrm{bub}}}{\Delta h_{\mathrm{LV}}} \tag{8}$$

The first term of the right side on the first line in Equation (5) corresponds to the thermal resistance caused by temperature glide. The numerator of second term expresses the interfacial mass transfer resistance caused by strong concentration gradient. C_{ir} is the empirical constant 3.5 determined from the present experimental results. The denominator of second term is equivalent to the flow boiling HTC. α_{cv} is the contribution to flow boiling HTC by forced convection calculated as,

$$\alpha_{cv} = F\alpha_{L\_Carnavos} \tag{9}$$

F is the Reynolds number factor named by Chen (1966). $\alpha_{L\_Carnavos}$ is the total liquid HTC given by the conventional Carnavos correlation (1979, 1980).

$$\begin{aligned}
&F = 1 + C_{cv}/X_{tt} \\
&C_{cv} = 10\left(Re_L \times 10^{-4}\right)^{-0.6}\left[1 - 0.93\exp\left(-4 \cdot Re_L \times 10^{-4}\right)\right]\left(\rho_V/\rho_L\right)^{0.35} \\
&\alpha_{L_Carnavos} = \frac{\lambda_L}{\left(d_{eq}/\eta_A\right)}0.023\left[\frac{G_r\left(1-x\right)\left(d_{eq}/\eta_A\right)}{\mu_L}\right]^{0.8}\mathrm{Pr}^{0.4} \times F_{Carnavos} \\
&F_{Carnavos} = \left(\frac{d_{eq}}{d_{max}}\right)^{0.2}\left(\frac{d_{max}}{d_{eq}\eta_A}\right)^{0.5}\left(\frac{1}{\cos\beta}\right)^{3}
\end{aligned} \tag{10}$$

Of the Reynolds number factor F, the coefficient C_{cv} is given from Mori et al. (2002) with an empirical modification from the large data set listed in Table 5. The Carnavos correlation $\alpha_{L\_Carnavos}$ is transcribed in Equation (8) with the geometrical parameters of the microfin tube listed in Table 1. Here, the liquid and vapor properties are represented by those properties locally evaluated at each mass fraction in the liquid and vapor determined by the phase equilibrium.

The other contribution of nucleate boiling, $\alpha_{nb,m}$, of the binary mixture is calculated by means of Thome (1983) to consider the reduction of the effective superheat at the boiling site. In the superheated sublayer adjacent to the tube wall surface, the more volatile component readily departs as the bubbles form and the less volatile component is enriched.

Thus, the bubble point temperature locally increases in the sublayer, and this reduces the effective superheat that is the actual driving temperature difference of boiling.

$$\alpha_{\mathrm{nb,m}} = \left(\frac{\tilde{X}_1}{\alpha_{\mathrm{nb},1}} + \frac{\tilde{X}_2}{\alpha_{\mathrm{nb},2}} \right)^{-1} \times N_{\mathrm{Sn}}{}^{\frac{7}{5}},$$
$$N_{\mathrm{Sn}} = \left[1 - \left(\tilde{Y}_1 - \tilde{X}_1 \right) \left(\frac{a_{\mathrm{L}}}{D_{12,\mathrm{L}}} \right)^{1/2} \left(\frac{Cp_{\mathrm{L}}}{\Delta h_{\mathrm{LV,L}}} \right) \left(\frac{dT_{\mathrm{bub}}}{d\tilde{X}_1} \right) \right]^{-1} \tag{11}$$

where, $\tilde{X}_1$ and $\tilde{X}_2$ are the mole fractions of the more and the less volatile components in the liquid. N_{Sn} is a dimensionless number called the Scriven number (Scriven, 1959; VanStralen, 1967) introduced by Claus and Leonidopoulos (1974), the very first prediction of the pool boiling HTC in binary liquids. $\left(dT_{\mathrm{bub}} / d\tilde{X}_1 \right)$ is the slope of the bubble temperature curve. The exponent 7/5 is analytically derived by Thome (1981) by consideration of the effect of the composition change in the thermal boundary layer stripping by departing bubbles. $\tilde{Y}_1$ is the mole fraction of the more volatile component in the vapor. a_{L} is the liquid thermal diffusivity. $D_{12,\mathrm{L}}$ is the mutual liquid diffusion coefficient calculated by the correlation of Vignes (1966), associated with the correlation of Wilke and Chang (1955) proposed for infinite dilutions. The ideal nucleate boiling HTCs of the more and the less volatile components, $\alpha_{\mathrm{nb},1}$ and $\alpha_{\mathrm{nb},2}$ are calculated by means of Momoki et al. (1995) for each component.

$$
\left.
\begin{aligned}
&\alpha_{\mathrm{nb}} = K^{0.745} S \alpha_{\mathrm{pb}} \\
&\alpha_{\mathrm{pb}} = C_{\mathrm{pb}} \left(\frac{\lambda_{\mathrm{L}}}{D_{\mathrm{be}}} \right) 207 \left[\frac{q_{\mathrm{act}} D_{\mathrm{be}}}{\lambda_{\mathrm{L}} \left(T_{\mathrm{sat}} + 273.15 \right)} \right]^{0.745} \left(\frac{\rho_{\mathrm{V}}}{\rho_{\mathrm{L}}} \right)^{0.581} \mathrm{Pr_L}^{0.533} \\
&K^{0.745} = \frac{q_{\mathrm{nb}}}{q} \cong \left(1 + 0.875\eta + 0.518\eta^2 - 0.159\eta^3 + 0.7907\eta^4 \right)^{-1} \\
&\eta = \frac{\alpha_{\mathrm{cv}}}{S \alpha_{\mathrm{pb}}}, \\
&S = \frac{1}{\zeta} \left(1 - e^{-\zeta} \right) \\
&\zeta = 10^{-5} \mathrm{Ja}^{*1.25} \mathrm{La} \left(\frac{\alpha_{\mathrm{cv}}}{\lambda_{\mathrm{L}}} \right) \\
&D_{\mathrm{be}} = 0.511 \cdot \mathrm{La} \\
&\mathrm{La} = \sqrt{\frac{2\sigma}{g \left(\rho_{\mathrm{L}} - \rho_{\mathrm{V}} \right)}} \\
&\mathrm{Ja}^{*} = \frac{\rho_{\mathrm{L}}}{\rho_{\mathrm{V}}} \frac{Cp_{\mathrm{L}} \left(T_{\mathrm{sat}} + 273.15 \right)}{\Delta h_{\mathrm{LV}}}
\end{aligned}
\right\} \qquad (12)
$$

α_{pb} is the pool boiling HTC of each component alone, given by Stephan and Abdelsalam correlation (1980) at the bulk pressure. C_{pb} was originally recommended as the value 2.8 for R123, R134a, and R22 boiling flow in a microfin tube of 8.37 mm ID by Momoki et al. (1995). This coefficient is supposed to be larger than the 1.35 that is obtained for flow boiling in smooth tubes by Takamatsu et al. (1993a) because swirling flow along the helical microfins expedites the departure of bubbles. Hence, this coefficient is here proposed as a function of the bubble Reynolds number, which is characterized with the reduced vapor velocity, $q/(\Delta h_{\mathrm{LV}} \rho_{\mathrm{V}})$, and the Laplace constant, La.

$$
C_{\mathrm{pb}} = 1.55 \mathrm{Re}_{\mathrm{bub}}^{-0.145}, \ \mathrm{Re}_{\mathrm{bub}} = \frac{q_{\mathrm{act}}}{\left(\Delta h_{\mathrm{LV}} \rho_{\mathrm{V}} \right)} \frac{\mathrm{La}}{\mu_{\mathrm{L}}} \qquad (13)
$$

This bubble Reynolds number was introduced by Rohsenow (1951) for nuclear boiling heat transfer. The coefficient 1.55 and the exponent -0.145 were empirically obtained from the data set listed in Table 5.

Figure 8 verifies the proposed prediction from Equations (5) to (9) for the tested binary mixture R32/R1234ze(E)

at an average saturation temperature of 10 °C, heat flux of 10 kW m^{-2}, and various mass velocities from 143 to 380 kg $m^{-2}s^{-1}$ (plotted against vapor quality). As shown in Figures 8 (b) and (c), excellent agreement for the proposed predictions is demonstrated with a high degree of overlap between the solid lines and symbols, for the experimental HTC at the circulation compositions 0.2/0.8 and 0.5/0.5 by mass. In Figures 8 (a) and (d), the verification is also shown for the varied circulation composition of R32 from 0 to 1 where indicates presence of the single components R1234ze(E) and R32. As shown with the overlap of solid lines and symbols in Figure 8, the proposed correlation predicts well HTC in the entire range of circulation composition.

3.5 Pressure drop of binary mixture R32/R1234ze(E)

Table 6 lists the comparison results on pressure drop for the single components R32 and R1234ze(E). The experimental results are compared with four selected correlations by Kubota et al. (2001), Newell and Shah (2001), Goto et al. (2001, 2007), and Filho et al. (2004). As shown in Table 6, the all selected correlations reasonably agree with the experimental results.

Figure 6 (a) compares the pressure drop of R32/R1234ze(E) 0.2/0.8 by mass between the experiment and the prediction at the average temperature of 10 °C, and mass velocities from 143 to 380 kg $m^{-2}s^{-1}$. Solid lines are the predicted pressure drop by the correlation of Kubota et al. (2001) proposed for other single components and azeotropic mixtures. Data from the present results of the zeotropic mixture and the solid lines of the correlation show good agreement.

Figure 9 (b) shows the variation of the pressure drop of R32/R1234ze(E) due to the circulation composition. In contrast to the HTC, the pressure moderately decreases from the composition range 0 to 1. The correlation shown by solid lines well predicts this tendency in the entire range of tested compositions. Mass transfer resistance, discussed in

the heat transfer model, appears to be negligible for the momentum dissipation. As mentioned above, the correlation proposed for single components and azeotropic mixtures predicts well the pressure drop for the mixture, when the liquid and vapor properties are substituted by the mixture properties evaluated at the local vapor quality and the circulation composition.

4. Conclusions

Flow boiling of the low GWP zeotropic mixture R32/R1234ze(E) in a horizontal microfin tube has been experimentally investigated. HTC of R32 alone is higher than that of R1234ze(E), mainly due to the higher liquid thermal conductivity and large latent heat of vaporization when comparing R32 to R1234ze(E). The mixture R32/R1234ze(E) yielded a significantly lower HTC than either of the single components by typical mass transfer resistance of zeotropic mixtures. HTC is minimized at the circulation composition of approximately 0.2/0.8 by mass, where the temperature glide and the mole fraction difference of the liquid to vapor are maximized. The experimental HTCs showed good agreement with several correlations for single components R32 and R1234ze(E). However, for the mixture R32/R1234ze(E), the deviations were considerably large. Based on the correlations of Stephan (1992), Momoki et al. (1995), and Thome (1983), a predicting correlation was proposed that considers the thermal resistance in the vapor phase due to the temperature glide and the boiling heat transfer degradation caused by the decrease in the effective superheat. Excellent agreement with the proposed prediction and the experimental HTC was obtained. The pressure drop of the binary mixture was well predicted by a correlation proposed for single components and azeotropic mixtures.

Acknowledgements

The work presented here was financially supported by the New Energy and Industrial Technology Development

Organization (NEDO). The test tubes were supplied from Kobelco and Materials Copper Tube, Ltd.

Appendices

A. Uncertainty analysis

Following Figure 3, procedure of the uncertainty analysis is hereinafter specified. The 95 % coverage of uncertainty propagated with several variables is obtained by means of the square-root rule (Taylor 1982; Moffat, 1988), assuming that the variables are independent and random.

A.1 Uncertainties in heat transfer rates

The heat transfer rates in the after heater and the subsections are obtained from the safe mathematical formula,

$$Q_{\mathrm{H2O}} = \rho_{\mathrm{H2O}} Cp_{\mathrm{H2O}} V_{\mathrm{H2O}} \left(T_{\mathrm{H2O,i}} - T_{\mathrm{H2O,o}} \right) - Q_{\mathrm{loss}} \qquad \text{(A.1)}$$

The uncertainty of water properties are negligible comparing to that of the other measured parameters. Hence the uncertainty of those heat transfer rates $U_{Q_{\mathrm{H2O,\,AH}}}$, $U_{Q_{\mathrm{H2O,\,1}}}$, $U_{Q_{\mathrm{H2O,\,2}}}$, $U_{Q_{\mathrm{H2O,\,3}}}$, and $U_{Q_{\mathrm{H2O,\,4}}}$ are determined by the same formula,

$$U_{Q_{\mathrm{H2O}}}{}^2 \approx \left[\rho_{\mathrm{H2O}} Cp_{\mathrm{H2O}} \left(T_{\mathrm{H2O,o}} - T_{\mathrm{H2O,i}} \right) \cdot U_{V_{\mathrm{H2O}}} \right]^2 + \left(V_{\mathrm{H2O}} \rho_{\mathrm{H2O}} Cp_{\mathrm{H2O}} \right)^2 \left(U_{T_{\mathrm{H2O,i}}}{}^2 + U_{T_{\mathrm{H2O,i}}}{}^2 \right) + U_{Q_{\mathrm{loss}}}{}^2 \qquad \text{(A.2)}$$

where, $U_{V_{\mathrm{H2O}}}$ and $U_{T_{\mathrm{H2O}}}$ are the uncertainty related to the volumetric flow meter and Pt resistance thermometer as listed in Table 2. $U_{Q_{\mathrm{loss}}}$ is the uncertainty in heat loss measured by the preliminary test (approximately 1.1 W).

A.2 Uncertainties in enthalpies

As described in Equation (1), the enthalpy changes through the after heater and the subsections are given as,

$$\Delta h = Q_{\mathrm{H2O}} / W_r \tag{A.3}$$

Hence the uncertainty in these enthalpy changes $U_{\Delta h_{\mathrm{AH}}}$, $U_{\Delta h_1}$, $U_{\Delta h_2}$, $U_{\Delta h_3}$, and $U_{\Delta h_4}$ are,

$$U_{\Delta h}{}^2 \approx \left(U_{Q_{\mathrm{H2O}}} / W_{\mathrm{r}}\right)^2 + \left(-U_{W_{\mathrm{r}}} / W_{\mathrm{r}}{}^2\right)^2 \tag{A.4}$$

where, $U_{W_{\mathrm{r}}}$ is the uncertainty related to the mass flow meter as listed in Table2. With the enthalpy change Δh, the local enthalpy can be expressed as,

$$\begin{aligned}
h_{\mathrm{AHo}} &= h_{\mathrm{AHo}}\left(P_{\mathrm{AHo}}, T_{\mathrm{AHo}}, X_{\mathrm{R32}}\right)_{\mathrm{equilibrium}} \\
h_1 &= h_{\mathrm{AHo}} - \Delta h_{\mathrm{AH}} \\
h_2 &= h_{\mathrm{AHo}} - \Delta h_{\mathrm{AH}} - \Delta h_1 \\
h_3 &= h_{\mathrm{AHo}} - \Delta h_{\mathrm{AH}} - \Delta h_1 - \Delta h_2 \\
h_4 &= h_{\mathrm{AHo}} - \Delta h_{\mathrm{AH}} - \Delta h_1 - \Delta h_2 - \Delta h_3 \\
h_5 &= h_{\mathrm{AHo}} - \Delta h_{\mathrm{AH}} - \Delta h_1 - \Delta h_2 - \Delta h_3 - \Delta h_4
\end{aligned} \tag{A.5}$$

When the uncertainty in the property database is negligible, the uncertainty in the enthalpy h_{AHo} can be calculated as the deviation between maximum and minimum enthalpies referring three measured parameters.

$$\begin{aligned}
U_{h_{\mathrm{AHo}}} &\approx \left(h_{\mathrm{AHo_max}} - h_{\mathrm{AHo_min}}\right)/2 \\
h_{\mathrm{AHo_max}} &= \mathrm{Max}\left[h_{\mathrm{AHo}}\left(P_{\mathrm{AHo}} \pm U_{P_{\mathrm{AHo}}}, T_{\mathrm{r,AHo}} \pm U_{T_{\mathrm{r,AHo}}}, X_{\mathrm{R32}} \pm U_{X_{\mathrm{R32}}}\right)_{\mathrm{equilibrium}}\right] \\
h_{\mathrm{AHo_min}} &= \mathrm{Min}\left[h_{\mathrm{AHo}}\left(P_{\mathrm{AHo}} \pm U_{P_{\mathrm{AHo}}}, T_{\mathrm{r,AHo}} \pm U_{T_{\mathrm{r,AHo}}}, X_{\mathrm{R32}} \pm U_{X_{\mathrm{R32}}}\right)_{\mathrm{equilibrium}}\right]
\end{aligned} \tag{A.6}$$

where $U_{P_{\mathrm{AHo}}}, U_{T_{\mathrm{r,AHo}}}$, and $U_{X_{\mathrm{R32}}}$ are the uncertainties related to the absolute pressure transducer, K type thermocouples, and the gas-chromatograph, respectively. With the basis of uncertainty $U_{h_{\mathrm{AHo}}}$, the uncertainties in the enthalpies from h_1 to h_5 are determined as follows.

$$
\begin{aligned}
U_{h_1}{}^2 &= U_{h_{\mathrm{AHo}}}{}^2 + U_{\Delta h_{\mathrm{AH}}}{}^2 \\
U_{h_2}{}^2 &= U_{h_{\mathrm{AHo}}}{}^2 + U_{\Delta h_{\mathrm{AH}}}{}^2 + U_{\Delta h_1}{}^2 \\
U_{h_3}{}^2 &= U_{h_{\mathrm{AHo}}}{}^2 + U_{\Delta h_{\mathrm{AH}}}{}^2 + U_{\Delta h_1}{}^2 + U_{\Delta h_2}{}^2 \\
U_{h_4}{}^2 &= U_{h_{\mathrm{AHo}}}{}^2 + U_{\Delta h_{\mathrm{AH}}}{}^2 + U_{\Delta h_1}{}^2 + U_{\Delta h_2}{}^2 + U_{\Delta h_3}{}^2 \\
U_{h_5}{}^2 &= U_{h_{\mathrm{AHo}}}{}^2 + U_{\Delta h_{\mathrm{AH}}}{}^2 + U_{\Delta h_1}{}^2 + U_{\Delta h_2}{}^2 + U_{\Delta h_3}{}^2 + U_{\Delta h_4}{}^2
\end{aligned}
\tag{A.7}
$$

A.3 Uncertainties in local pressures

The uncertainties in local pressures are obtained as the combination of uncertainties in the absolute pressure P_0 and the differential pressure ΔP.

$$
\begin{aligned}
U_{P_{\mathrm{AHi}}}{}^2 &= U_{P_0}{}^2 + U_{\Delta P_{01}}{}^2 \\
U_{P_2}{}^2 &= U_{P_0}{}^2 + U_{\Delta P_{02}}{}^2 \\
&\vdots \\
U_{P_5}{}^2 &= U_{P_0}{}^2 + U_{\Delta P_{05}}{}^2
\end{aligned}
\tag{A.8}
$$

A.4 Uncertainties in representative refrigerant temperatures

As described in Equation (2), the arithmetic mean of the inlet and outlet temperatures represents the refrigerant temperature in a subsection. Thus, the uncertainty in the representative refrigerant temperature is the combination of the uncertainties in the inlet and outlet refrigerant temperatures. For the subsection 1, this is obtained as,

$$
U_{T_{\mathrm{r},1}}{}^2 \approx \left(U_{T_{\mathrm{r},1\mathrm{i}}}{}^2 + U_{T_{\mathrm{r},1\mathrm{o}}}{}^2 \right) \Big/ 2 \tag{A.9}
$$

The uncertainty in each refrigerant temperature can be calculated with the reference to three measured parameters.

$$
\begin{aligned}
U_{T_{\mathrm{r},1}} &\approx \left(T_{\mathrm{r},1\_\max} - T_{\mathrm{r},1\_\min} \right) \Big/ 2 \\
T_{\mathrm{r},1\_\max} &= \mathrm{Max} \left[T_{\mathrm{r},1} \left(P_{\mathrm{AHi}} \pm U_{P_{\mathrm{AHi}}}, h_1 \pm U_{h_1}, X_{\mathrm{R32}} \pm U_{X_{\mathrm{R32}}} \right)_{\mathrm{equilibrium}} \right] \\
T_{\mathrm{r},1\_\min} &= \mathrm{Min} \left[T_{\mathrm{r},1} \left(P_{\mathrm{AHi}} \pm U_{P_{\mathrm{AHi}}}, h_1 \pm U_{h_1}, X_{\mathrm{R32}} \pm U_{X_{\mathrm{R32}}} \right)_{\mathrm{equilibrium}} \right]
\end{aligned}
\tag{A.10}
$$

A.5 Uncertainties in tube wall temperature

The interior tube wall temperature T_{wi} is given as Equation (4). Thus, the uncertainty in the tube wall temperature is,

$$U_{T_{\mathrm{wi}}}{}^2 \approx \frac{\left(U_{T_{\mathrm{wo,\,top}}}{}^2 + U_{T_{\mathrm{wo,\,bottom}}}{}^2 + U_{T_{\mathrm{wo,\,right}}}{}^2 + U_{T_{\mathrm{wo,\,left}}}{}^2\right)}{4} + \left(\frac{Q_{\mathrm{H2O}}}{2\pi\lambda_{\mathrm{tube}}\Delta Z_\alpha}\right)^2\left[\left(\frac{U_{D_o}}{D_{\mathrm{o}}}\right)^2 + \left(\frac{U_{d_{\mathrm{eq}}}}{d_{\mathrm{eq}}}\right)^2\right] + \left[\ln\left(\frac{D_{\mathrm{o}}}{d_{\mathrm{eq}}}\right)\right]^2\left[\left(\frac{U_{Q_{\mathrm{H2O}}}}{2\pi\lambda_{\mathrm{tube}}\Delta Z_\alpha}\right)^2 + \left(\frac{-Q_{\mathrm{H2O}}}{2\pi\lambda_{\mathrm{tube}}{}^2\Delta Z_\alpha}U_{\lambda_{\mathrm{tube}}}\right)^2 + \left(\frac{-Q_{\mathrm{H2O}}}{2\pi\lambda_{\mathrm{tube}}\Delta Z_\alpha{}^2}U_{\Delta Z_\alpha}\right)^2\right] \quad \text{(A.11)}$$

where $U_{T_{\mathrm{wo,\,top}}}$, $U_{T_{\mathrm{wo,\,bottom}}}$, $U_{T_{\mathrm{wo,\,right}}}$, and $U_{T_{\mathrm{wo,\,left}}}$ are the uncertainties in the exterior tube wall temperatures related to the T type thermocouples as listed in Table 2. U_{D_o}, $U_{d_{\mathrm{eq}}}$, and $U_{\Delta Z_\alpha}$ are the uncertainties in the outer diameter, the equivalent inner diameter, and the active heating length of the test tube. Here those uncertainties U_{D_o}, $U_{d_{\mathrm{eq}}}$, and $U_{\Delta Z_\alpha}$ were given as 0.05 mm, 0.25mm, and 5 mm, respectively.

A.6 Uncertainties in heat fluxes

The uncertainties in heat fluxes based on the actual heat transfer area are determined as,

$$U_{q_{\mathrm{act}}}{}^2 \approx \left(\frac{U_{Q_{\mathrm{H2O}}}}{d_{\mathrm{eq}}\pi\eta_{\mathrm{A}}\Delta Z_\alpha}\right)^2 + \left(\frac{Q_{\mathrm{H2O}}}{d_{\mathrm{eq}}\pi\eta_{\mathrm{A}}\Delta Z_\alpha}\right)^2\left[\left(\frac{U_{d_{\mathrm{eq}}}}{d_{\mathrm{eq}}}\right)^2 + \left(\frac{U_{\eta_{\mathrm{A}}}}{\eta_{\mathrm{A}}}\right)^2 + \left(\frac{U_{\Delta Z_\alpha}}{\Delta Z_\alpha}\right)^2\right] \quad \text{(A.12)}$$

where $U_{\eta_{\mathrm{A}}}$ is the uncertainty in the surface enlargement ratio on the test tube 0.05.

A.7 Uncertainties in HTC

From above, the uncertainties in average HTCs are determined as,

$$U_\alpha{}^2 \approx \left(\frac{U_{q_{\mathrm{act}}}}{T_{\mathrm{wi}} - T_{\mathrm{r}}}\right)^2 + \left[\frac{-U_{T_{\mathrm{wi}}}}{\left(T_{\mathrm{wi}} - T_{\mathrm{r}}\right)^2}\right]^2 + \left[\frac{-U_{T_{\mathrm{r}}}}{\left(T_{\mathrm{wi}} - T_{\mathrm{r}}\right)^2}\right]^2 \quad \text{(A.13)}$$

The uncertainty U_α predominantly depends on the temperature difference between tube wall and refrigerant (T_{wi} - T_{r}) and widely ranged from 0.08 to 135 kW $\mathrm{m^{-2}K^{-1}}$ in the entire range of test condition. Therefore, the experimentally

determined HTCs associating with the large uncertainty were eliminated. For each experimental HTC, the uncertainty is plotted with horizontal bar in Figures 5 and 8.

A.8 Uncertainties in pressure drops

From Equation (5), the uncertainties in pressure drop $U_{\Delta P/\Delta Z}$ of each subsection are obtained as,

$$\begin{aligned} U_{(\Delta P/\Delta Z)_1}{}^2 &\approx \left(\frac{U_{\Delta P_{02}}}{\Delta Z_{\mathrm{DP},1}}\right)^2 + \left(-\frac{U_{\Delta P_{01}}}{\Delta Z_{\mathrm{DP},1}}\right)^2 + \left[\left(\frac{\Delta P_{02}-\Delta P_{01}}{\Delta Z_{\mathrm{DP},1}{}^2}\right)U_{\Delta Z_{\mathrm{DP},1}}\right]^2 \\ &\vdots \\ U_{(\Delta P/\Delta Z)_4}{}^2 &\approx \left(\frac{U_{\Delta P_{00}}}{\Delta Z_{\mathrm{DP},4}}\right)^2 + \left(-\frac{U_{\Delta P_{04}}}{\Delta Z_{\mathrm{DP},4}}\right)^2 + \left[\left(\frac{\Delta P_{00}-\Delta P_{04}}{\Delta Z_{\mathrm{DP},4}{}^2}\right)U_{\Delta Z_{\mathrm{DP},4}}\right]^2 \end{aligned} \tag{A.14}$$

where $U_{\Delta P_{00}} \ldots U_{\Delta P_{00}}$ are the uncertainties related to the differential pressure transducer, 0.3 kPa. $U_{\Delta Z_{\mathrm{DP},1}} \ldots U_{\Delta Z_{\mathrm{DP},4}}$ are the uncertainties in the intervals of pressure ports, 0.005 m. Typically, when the pressure drop is 20 kPa/m, the propagated uncertainty in the pressure drop ($\Delta P/\Delta Z$) is ± 0.78 kPa/m that is approximately 4% of the obtained value. For each experimentally determined pressure drop, the uncertainty is plotted with horizontal bar in Figure 9.

References

Akasaka, R., 2012. private communication, Department of Mechanical Engineering, Kyushu Sangyo University.

Butterworth, D., 1981. Unsolved problems in heat exchanger design. Heat Exchangers: Thermal-Hydraulic Fundamentals and Design. Edited by Kakac, S., Bergles, A. E., Mayinger. F., Hemisphere, Washington, 1093-1096.

Carnavos, T.C., 1979. Cooling air in turbulent flow with internally finned tubes. Heat Transfer Eng. 1 (2), 41-46.

Carnavos, T.C., 1980. Heat transfer performance of internally finned tubes in turbulent flow. Heat Transfer Eng. 1 (4), 32-37.

Cavalllini, A., DelCol, D., Longo, G.A., Rosset, L., 1998. Refrigerant vaporization inside enhanced tubes. In: Proc. Heat Transfer in Condensation and Evaporation: Eurotherm seminar, Grenoble, France, 222-231.

Celata, G.P., Cumo, M., Setaro, T., 1994. A review of pool and forced convective boiling of binary mixtures. Exp. Therm. Fluid Sci. 9, 367-381.

Chamra, L.M., Mago, P.J., 2007. Modelling of evaporation heat transfer of pure refrigerants and refrigerant mixtures in microfin tubes. Proc. IMechE., 221, Part C: J. Mechanical Engineering Science, 443-454.

Chen, J.C., 1966. Correlation for boiling heat transfer to saturated fluids in convective flow. I&EC Process Design and Development. 5 (3), 322-329.

Cho, J. M., Kim, Y.J., Kim, M.S., 2010. Experimental studies on the characteristics of evaporative heat transfer and pressure drop of CO_2/propane mixtures in horizontal and vertical smooth and microfin tubes. Int. J. Refrig. 33, 170-179.

Claus, W.F., Leonidopoulos, D.J., 1974. Pool boiling-binary liquid mixtures. Int. J. Heat Mass Transfer 17, 249-256.

Filho, E.P.B., Jabardo, J.M.S., Barbieri, P.E.L., 2004.Convective boiling pressure drop of refrigerant R-134a in horizontal smooth and microfin tubes. Int. J. Refrig. 27 (8), 895-903.

Fukuda, S., Takata, N., Koyama, S., 2012. The circulation composition characteristic of the zeotropic mixture R1234ze(E)/R32 in a heat pump cycle. In: Proc. Int. Refrigeration and Air Conditioning Conf. at Purdue, West Lafayette, IN, no. 2229, 1-8.

Goto, M., Inoue, N., Ishiwatari, N., 2001. Condensation and evaporation heat transfer of R410A inside internally grooved horizontal tubes. Int. J. Refrig., 24 (7), 628-638.

Goto, M., Inoue, N., Ishiwatari, N., 2007. Answer to comments by M.M. Awad on “Condensation and evaporation heat transfer of R410A inside internally grooved horizontal tubes”. Int. J. Refrig., 30 (8), 1467.

Haberschill, P., Gay, L., Aubouin, P., Lallemand, M., 2002. Performance prediction of a refrigerating machine using R-407C: the effect of the circulation composition on system performance. Int. J. Energy Res. 26, 1295-1311.

Hossain, M.A., Onaka, Y., Afroz, H.M.M., Miyara, A., 2013. Heat transfer during evaporation of R1234ze(E), R32, R410A and a mixture of R1234ze(E) and R32 inside a horizontal smooth tube. Int. J. Refrig. 36, 465-477.

Jakobs, R., Kruse, H., 1978. The use of non-azeotropic refrigerant mixture in heat pumps for energy saving. In: Proc. IIR Commissions B2, Delft, Netherlands, 207-218.

Jung, D., Radermacher, R., 1993. Prediction of evaporation heat transfer coefficient and pressure drop of refrigerant mixtures in horizontal tubes. Int. J. Refrig. 16 (3), 201-209.

Jung, D.S., McLinden, M., Radermacher, R., Didion, D., 1989a. Horizontal flow boiling heat transfer experiments with a mixture of R22/R114. Int. J. Heat Mass Transfer 32 (1), 131-145.

Jung, D.S., McLinden, M., Radermacher, R., Didion, D., 1989b. A study of flow boiling heat transfer with refrigerant mixtures. Int. J. Heat Mass Transfer 32 (9), 1751-1764.

Kandlikar, S. G., 1998a. Boiling heat transfer with binary mixtures: Part I- A theoretical model for pool boiling. Trans. ASME, J. Heat Transfer 120 (2), 380-387.

Kandlikar, S. G., 1998b. Boiling heat transfer with binary mixtures: Part II- flow boiling in plain tubes. Trans. ASME, J. Heat Transfer 120 (2), 388-395.

Kondou, C., 2008. A Study of CO_2 - air cross-finned heat exchangers. Ph. D. thesis, Kyushu University, Fukuoka, Japan.

Koyama, S., Matsuo, Y., Fukuda S, Akasaka, R. 2010b. Measurement of vapor-liquid equilibrium of HFO-1234ze(E)

/HFC-32. In: Proc. 2010 JSRAE Annual Conf., Kanazawa, Japan, 195-196 (in Japanese).

Koyama, S., Miyara, A., Takamatsu, H., Yonemoto, K., Fujii, T., 1987. Condensation and evaporation of non-azeotropic refrigerant mixtures of R22 and R114 inside a spirally grooved horizontal tube. The reports of Institute of Advanced Material Study Kyushu University 1 (1), 57-75 (in Japanese).

Koyama, S., Takata, N., Fukuda, S., 2010a. Drop-in experiments on heat pump cycle using HFO-1234ze(E) and its mixtures with HFC-32. In: Proc. Int. Refrigeration and Air Conditioning Conf. at Purdue, West Lafayette, IN, no. 2514, 1-8.

Kubota, A., Uchida, M., Shikazono, N., 2001. Predicting equations for evaporation pressure drop inside horizontal smooth and grooved tubes. Trans. JSRAE, 18 (4), 393-401(in Japanese).

Kuo, C.S., Wang, C.C., 1996. Horizontal flow boiling of R22 and R407C in a 9.52 mm micro-fin tube. Appl. Therm. Eng. 16, 719-731.

Lemmon, E.W., Huber, M.L., McLinden, M.O., 2010. Reference fluid thermodynamic and transport properties-REFPROP Ver. 9.0. National Institute of Standards and Technology, Boulder, CO, USA.

McLinden, M.O. and Radermacher, R., 1987. Mothod for comparing the performance of pure and mixed refrigerants in the vapour compression cycle. Int. J. Refrig. 10, 318-325.

Moffat, R.J., 1988. Description uncertainties in experimental results. Exp. Therm. Fluid Sci. 1, 3-17.

Momoki, S., Yu, J., Koyama, S., Fujii, T., Honda, H., 1995. A correlation for forced convective boiling heat transfer of refrigerants in a microfin tube. Trans. JAR, 12 (2), 177-184 (in Japanese).

Mori, H., Yoshida, S., Koyama, S., Miyara, A., Momoki, S., 2002. Prediction of heat transfer coefficients for refrigerants flowing in horizontal spirally grooved evaporator tubes. In: Proc. 14th JSRAE Annual Conf., 97-100, (in Japanese).

Murata K., Hashizume, K., 1993. Forced convective boiling of nonazeotropic refrigerant mixtures inside tubes. Trans. ASME, J. Heat Transfer 115, 680-689.

Murata, K., 1996. Correlation for forced convective boiling heat transfer of binary refrigerant mixtures -2nd report: a spirally grooved tube. Trans. JSME (B), 62 (599), 2723-2728 (in Japanese).

Newell, T.A., Shah, R.K., 2001. An assessment of refrigerant heat transfer, pressure drop, and void fraction effects in microfin tubes. HVAC&R Research, 7(2), 125-153.

Niederkrüger, M., Steiner, D., Shlünder, E.U., 1992. Horizontal flow boiling experiments of saturated pure components and mixtures of R546-R12 at high pressures. Int. J. Refrig. 15 (1), 48-58.

Niederküger, M., Steiner, D., 1994. Flow boiling heat transfer to saturated pure components and non-azeotropic mixtures in a horizontal tube. Chem. Eng. Prog. 33, 261-275.

Ohishi, K., Mori, H., Doi, H., Yoshida, S., 2004. Heat transfer to refrigerant R410A flowing in a horizontal spirally-grooved evaporator tube. In: Proc. 57th JSME Kyushu Branch Annual Conf. 48 (1), 123-124 (in Japanese).

Rohsenow, W.M., 1951. A method of correlating heat transfer data for surface boiling of liquids. In: Technical Report, Massachusetts Institute of Technology, Heat Transfer Laboratory 5, 1-15.

Ross, H., Radermacher, R., DiMarzo, M., Didion, D, 1987. Horizontal flow boiling of pure and mixed refrigerants, Int. J. Heat Mass Transfer, Vol. 30, no. 5, 979-992.

Schael, A.E., Kind, M., 2005. Flow pattern and heat transfer characteristics during flow boiling of CO_2 in a horizontal micro fin tube and comparison with smooth tube data. Int. J., Refrig. 28, 1186-1195.

Scriven, L.E., 1959. On the dynamics of phase growth. Chem. Engng. Sci. 10 (1), 1-13.

Shin, J.Y., Kim, M.S., Ro, S.T., 1997. Experimental study on forced convective boiling heat transfer of pure refrigerants and refrigerant mixtures in a horizontal tube. Int. J. Refrig. 20 (4), 267-275.

Spindler, K., Müller-Steinhagen, H., 2009. Flow boiling heat transfer of R134a and R404A in a microfin tube at low mass fluxes and low heat fluxes. Heat Mass Transfer 45, 967–977.

Stephan, K., 1992. Heat transfer in condensation and boiling. Translated by Green, C.V., Springer-Verlag, Berlin, Heidelberg, 286-291.

Stephan, K., Abdelsalam, M., 1980. Heat transfer correlations for natural convection boiling. Int. J. Heat Mass Transfer 23, 73-87.

Takamatsu, H., Momoki, S., Fujii, T., 1993a. A correlation for forced convective boiling heat transfer of pure refrigerants in a horizontal smooth tube. Int. J. Heat Mass Transfer 36 (13), 3351-3360.

Takamatsu, H., Momoki, S., Fujii, T., 1993b. A correlation for forced convective boiling heat transfer of nonazeotropic refrigerant mixture of HCFC22/CFC114 in a horizontal smooth tube. Int. J. Heat Mass Transfer 36 (14), 3555-3563.

Taylor, J.T., 1982. An introduction to error analysis, second ed. University science book.

Thome, J.R., 1981. Nuclear pool boiling of binary liquids-an analysis equation. AIChE. Symp. Ser. 77 (208), 238-250.

Thome, J.R., 1983. Prediction of binary mixture boiling heat transfer coefficients using only phase equilibrium data. Int. J. Heat Mass Transfer 26 (7), 965-974.

Thome, J.R., Kattan, N., Favrat, D., 1997. Evaporation in microfin tubes: a generalized prediction model. In: Proc. Convective Flow and Pool Boiling Conf., Kloster Irsee, Germany, Paper VII-4.

Torikoshi, K., and Ebisu, T., 1994. In-tube heat transfer characteristics of refrigerant mixtures of HFC-32/134a and HFC-32/125/134a. In: Proc. Int. Refrigeration and Air Conditioning Conf., West Lafayette, IN, 293-298.

VanStralen, S.J.D., 1967. Bubble growth rate in boiling binary mixtures. Br. Chem. Engng. 12 (3), 390-394.

Vignes, A., 1966. Diffusion in binary solutions. Ind. Eng. Chem. Fundam. 5 (2), 189-199.

Wettermann, M., Steiner, D., 2000. Flow boiling heat transfer characteristics of wide-boiling mixtures. Int. J. Therm. Sci. 39, 225-235.

Wilke, C. R., Chang, P., 1955. Correlation of diffusion coefficients in dilute solutions. AIChE. J., 1 (2), 264-270.

Yoshida, S., Hong, H.P., Mori, H., 1993. Enhancement of heat transfer to non-azeotropic refrigerant mixture in a horizontal, spirally grooved evaporator tube. Trans. JSME (B), 59 (560), 283-288 (in Japanese).

Yoshida, S., Matsunaga, T., Hong, H.P., Nishikawa, K., 1988. Heat transfer enhancement in horizontal spirally grooved evaporator tubes. JSME Int. J., Ser. II, 31 (3), 505-512.

Yoshida, S., Matsunaga, T., Mori, H., Ohishi, K., 1990. Heat transfer to non-azeotropic mixtures of refrigerants flowing in a horizontal evaporator tube. Trans. JSME (B), 56 (524), 198-203 (in Japanese).

Yu, J., Koyama, S., Momoki, S., 1995. Experimental study of flow boiling heat transfer in a horizontal microfin tube. The reports of Institute of Advanced Material Study Kyushu University, 9 (1), 27-42.

Yun, R., Kim, Y., Seo, K., Kim, H.Y., 2002. A generalized correlation for evaporation heat transfer of refrigerants in micro-fin tubes. Int. J. Heat Mass Transfer, 45, 2003-2010.

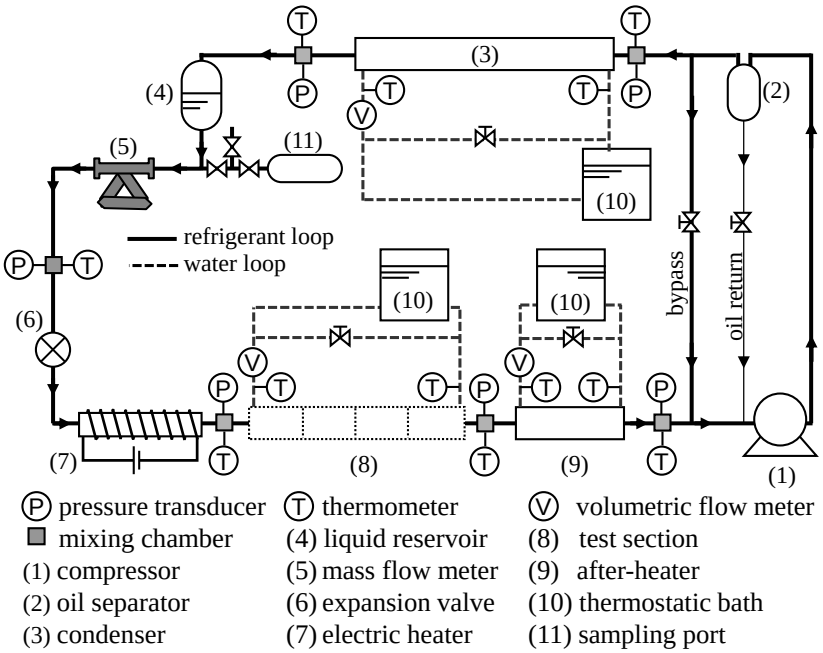

Figure 1 Experimental apparatus.

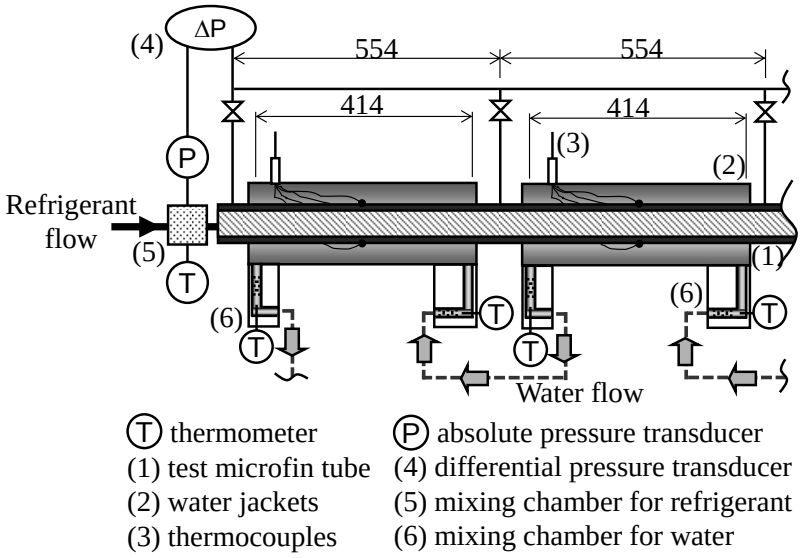

Figure 2 Two subsections placed upstream in the test section.

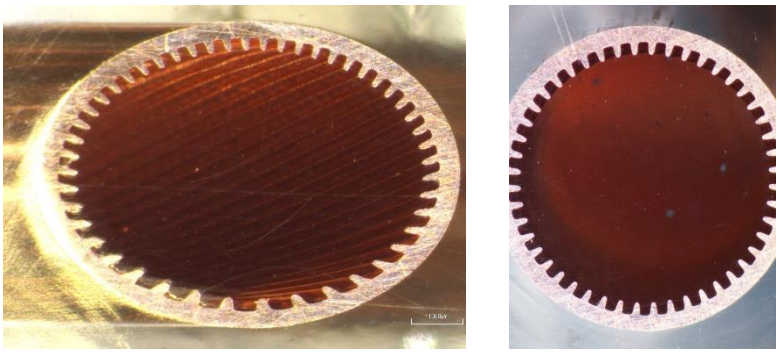

(a) 45 degree cut surface (b) perpendicular cut surface

Figure 3 Microscopic cross-sectional area of the test tube.

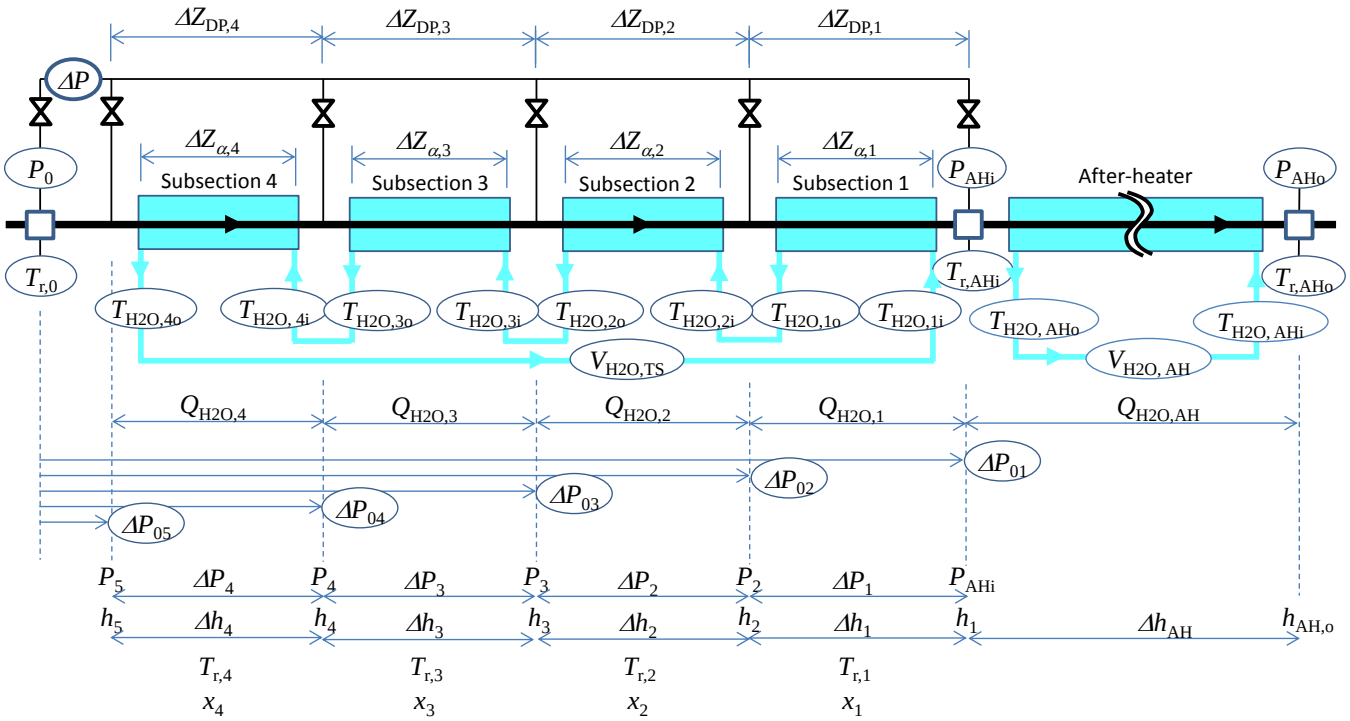

Figure 4 Data reduction procedure (Circled notations indicate the measured values).

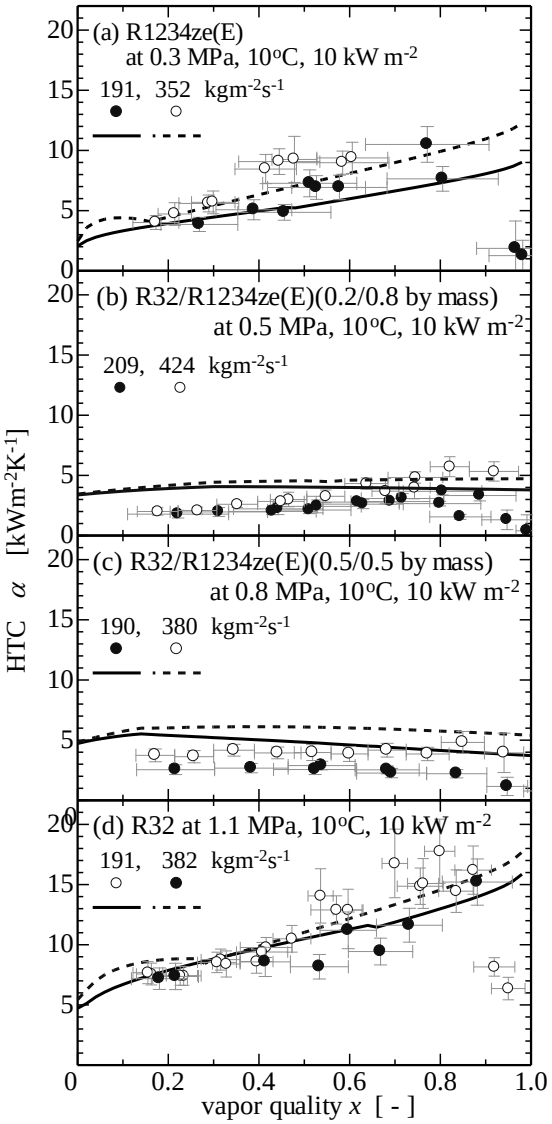

Figure 5 Measured HTC and predicted HTC by existing correlations for four different compositions.

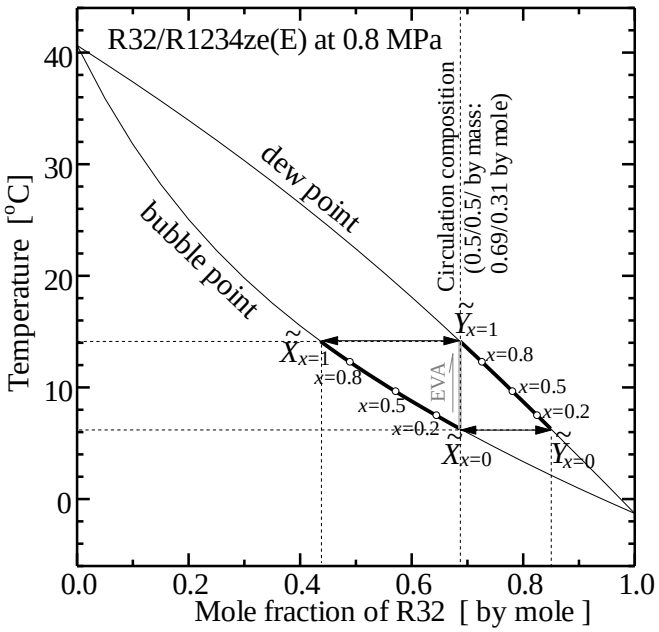

Figure 6 Phase equilibria of R32/R1234ze(E) at 0.8 MPa calculated by Refprop coupled with the mixing parameters optimized by Akasaka (2012) to the measured PvT data by Koyama et al. (2010b).

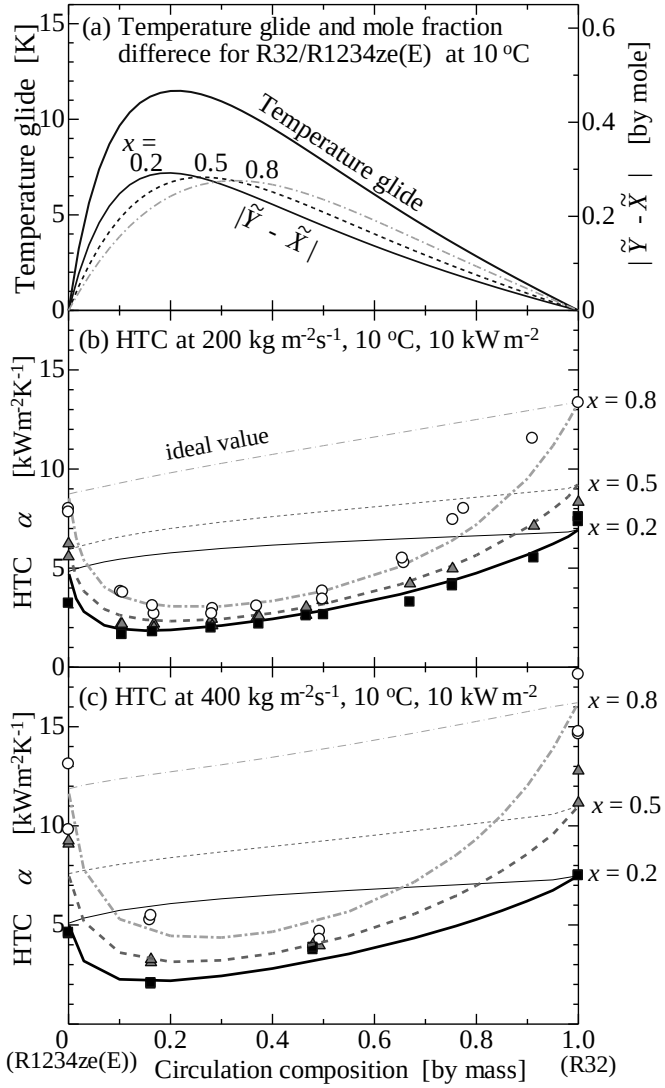

Figure 7 Effect of the temperature glide and mole fraction difference on HTC degradation.

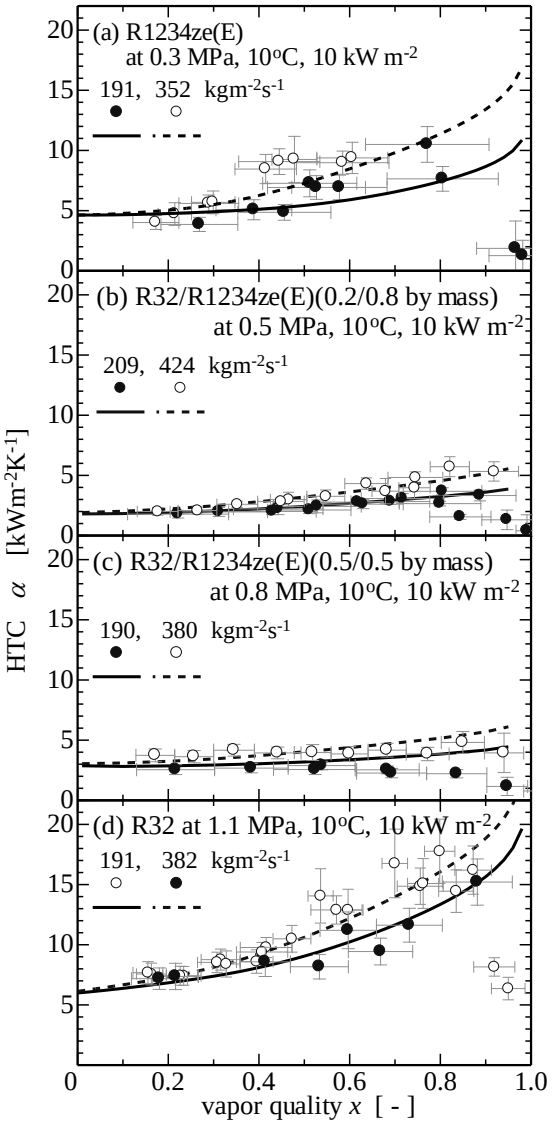

Figure 8 Comparison between the measured HTC and the proposed correlation.

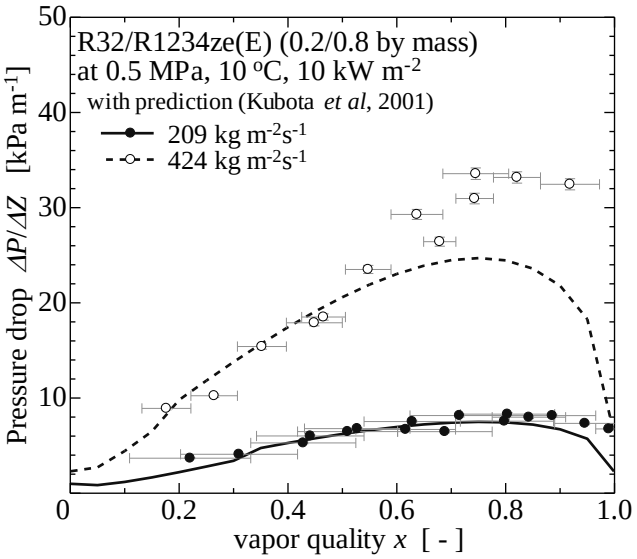

(a) variation of pressure drop against vapor quality at 0.2/0.8 by mass

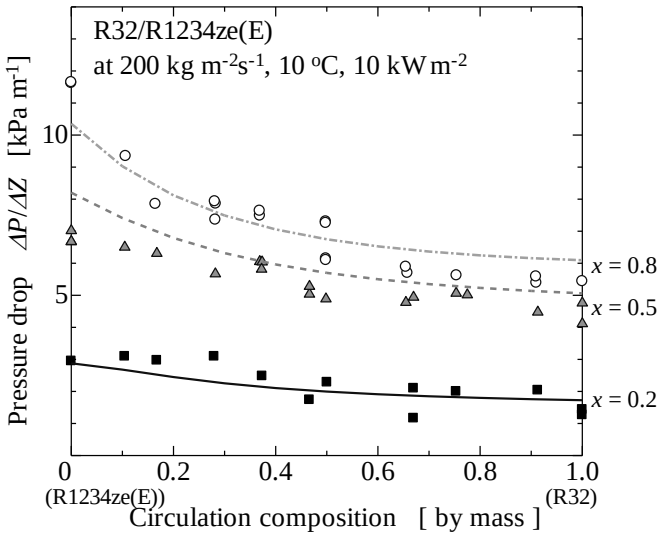

(b) effect of circulation composition

Figure 9 Pressure drop of binary mixture R32/R1234ze(E).

Figure Captions

Figure 1 Experimental apparatus

Figure 2 Two subsections placed upstream in the test section

Figure 3 Microscopic cross-sectional area of the test tube.

(a) 45 degree cut surface (b) perpendicular cut surface

Figure 4 Data reduction procedure (Circled notations indicate the measured values).

Figure 5 Measured HTC and predicted HTC by existing correlations for four different compositions.

Figure 6 Phase equilibria of R32/R1234ze(E) at 0.8 MPa calculated by Refprop coupled with the mixing parameters optimized by Akasaka (2012) to the measured PvT data by Koyama et al. (2010b).

Figure 7 Effect of the temperature glide and mole fraction difference on HTC degradation.

Figure 8 Comparison between the measured HTC and the proposed correlation.

Figure 9 Pressure drop of binary mixture R32/R1234ze(E).

Table 1 Dimensions of the test microfin tube.

outer diameter	D_o	6.04	mm
fin root diameter	d_{max}	5.45	mm
equivalent inner diameter	d_{eq}	5.35	mm
fin height	h_{fin}	0.255	mm
helix angle	β	20.1	o
number of fins	N_{fin}	48	-
surface enlargement	η_A	2.24	-

Table 2 Measurement uncertainties.

measurement points		instruments, max. reading (model)	uncertainty
refrig. temp.	U_{T_r}	K type T.C., ϕ 1 mm (Yamari, KS1.0ϕ200 316 L)	±0.05 °C
refrig. flow rate	U_{W_r}	mass flow meter, Max. 50 kg h^{-1} (Oval ALTI mass, CA003L)	±0.05 kg h^{-1} (0.1% of reading, zero stability; 0.0072 kg h^{-1})
refrig. absolute pressure	U_P	absolute pressure transducer, Max. 1 MPa$_{abs}$ (Kyowa PHS-10KA)	± 2 kPa (0.2% of reading)
refrig. differential pressure	$U_{\Delta P}$	differential pressure transducer, Max. ±100 kPa (Kyowa PD-1KA)	±0.3 kPa (0.3% of reading)
refrig. composition	$U_{X_{R32}}$	gas-chromatograph, TCD type (J-Science Lab, GC7100-T, On-column, Career gas – He)	±0.03 by mass
tube wall temp.	$U_{T_{wo}}$	T type T.C., ϕ 0.127 mm (Ishikawa Trading Co., LTD., TFCP-005, TFCC-005)	±0.05 °C
water temp.	$U_{T_{H2O}}$	Pt resistance thermometer, ϕ 2.0 mm (Yamari Resistance Bulb, PT100Ω(s)4W-1mA classA)	±0.03 °C
water flow rate	$U_{V_{H2O}}$	volumetric flow meter, Max. 300 L h^{-1} (Oval, ECO OVAL, LGV45A30)	±1.5 L h^{-1} (0.5% of reading)

Table 3 Assessment of the experimental HTC and selected correlations for single components R1234ze(E) and R32.

	R1234ze (E)		R32	
	$\bar{\varepsilon}$	σ_{dev}	$\bar{\varepsilon}$	σ_{dev}
Momoki et al. (1995)	0.11	0.36	-0.04	0.23
Thome et al. (1997)	0.18	0.46	0.02	0.18
Mori et al. (2002)	0.13	0.45	-0.01	0.17
Yun et al. (2002)	-0.41	0.33	-0.04	0.31
Chamra and Mago (2007)	0.92	0.92	1.01	0.51
Murata (1996)	-0.41	0.30	0.16	0.30
Cavallini et al. (1998)	0.20	0.58	0.20	0.24

Table 4 Assessment of the experimental HTC and selected correlations for the mixture R32/R1234ze(E).

	R32/R1234ze (E)	
	$\bar{\varepsilon}$	σ_{dev}
Murata (1996)	2.64	4.70
Cavallini et al. (1998)	0.54	0.42
Chamra and Mago. (2007)	-0.14	0.33

Table 5 Ranges of the experimental conditions of the data sources for single component flow boiling.

	Refrigerant	P [MPa]	G_r [kg m^{-2}s^{-1}]	$q_{act}h_A$ [kW m^{-2}]	d_{eq} or d_{max} [mm]
Yoshida et al. (1988)	R22	0.4 - 0.59	50 - 300	5.1 - 10.2	(d_{eq}) 11.6
Yu et al. (1995)	R22	0.66 - 1.22	115- 395	- 88	(d_{eq}) 8.14
	R123	0.25 - 0.45	113 - 309	- 58	
	R134a	0.56- 1.22	209 – 357	- 38	
Schael and Kind (2005)	R744	3.97	75 - 500	4 - 120	(d_{max}) 8.62
Spindler and Müller-Steinhagen (2009)	134a	0.13 - 0.41	20 - 150	1 - 15	(d_{max}) 8.92
Kondou (2008)	R744	3.5 - 5.0	200 - 460	9 - 24	(d_{eq}) 5.67
Ohishi et al. (2004)	R410A	0.93	100 - 500	10	(d_{eq}) 4.26
Kuo and Wang (1996)	R22	0.6	318	6 - 14	(d_{max}) 8.92
Present data	R32	0.88 – 1.1	141 - 360	4.5 - 40	(d_{eq}) 5.35
	R1234ze(E)	0.28 – 0.3	140 - 385	13 - 34	

Table 6 Assessment of the experimental pressure drop and selected correlations for single components R1234ze(E) and R32.

	R1234ze (E)		R32	
	$\bar{\varepsilon}$	σ_{dev}	$\bar{\varepsilon}$	σ_{dev}
Kubota *et al*. (2001)	0.18	0.19	0.21	0.23
Newell and Shah (2001)	0.60	0.35	0.04	0.23
Goto *et al*. (2001, 2007)	-0.32	0.15	-0.18	0.16
Filho *et al*. (2004)	-0.12	0.13	-0.08	0.23